

Optimal mixture of randomly dispersed quantum dots for optical excitation transfer via optical near-field interactions

Makoto Naruse,^{1,2} Tadashi Kawazoe,² Ryuichi Ohta,² Wataru Nomura,² and Motoichi Ohtsu²

¹*National Institute of Information and Communications Technology, 4-2-1 Nukui-kita, Koganei, Tokyo 184-8795, Japan*

²*Department of Electrical Engineering and Information Systems and Nanophotonics Research Center, School of Engineering, The University of Tokyo, 2-11-16 Yayoi, Bunkyo-ku, Tokyo 113-8656, Japan*

(Received 2 June 2009; revised manuscript received 26 July 2009; published 22 September 2009)

We theoretically and experimentally investigated a system composed of a mixture of different-sized quantum dots involving optical near-field interactions to effectively induce optical excitation transfer. We demonstrated that the ratio of the number of smaller quantum dots to larger ones can be optimized using a density-matrix formalism so that excitons generated in the smaller ones are efficiently transferred to the larger ones. We also describe experimental demonstrations based on a mixture of 2 nm- and 2.8 nm-diameter CdSe/ZnS quantum dots dispersed on the surface of a silicon photodiode, where the increase in induced photocurrents due to optical excitation transfer is maximized at a certain quantum dot mixture which agrees with theoretical calculations.

DOI: [10.1103/PhysRevB.80.125325](https://doi.org/10.1103/PhysRevB.80.125325)

PACS number(s): 74.25.Gz, 78.67.Bf, 73.63.Kv

I. INTRODUCTION

There have been in-depth theoretical and experimental efforts to reveal and exploit light-matter interactions on the nanometer scale¹⁻³ because of their potential impact in a wide range of applications. Since they are based on optical near-field interactions, quantitative breakthroughs have been achieved, such as in overcoming the integration restrictions posed by conventional propagating light.⁴ Moreover, qualitative innovations are made possible by the unique attributes of optical near-field interactions which are unachievable by their conventional counterparts.^{1,5}

One such unique function is the optical excitation transfer between nanoscale matter via optical near-field interactions.⁶ The localized nature of optical near fields at the surface of nanoscale matter could free us from conventional optical selection rules, meaning that optical excitation could be excited to energy levels that are conventionally dipole forbidden.¹ This unique behavior of optical near-field interactions has been theoretically formulated as the dressed photon model.^{1,7,8} Also, it has already been demonstrated experimentally in CuCl quantum dots,⁶ InAs quantum dots,⁹ and ZnO nanorods.¹⁰ Its application to logic devices^{11,12} and information and communication systems⁵ has also been demonstrated. The process of optical excitation transfer has also been extensively studied in artificial photosynthesis systems.^{13,14}

Besides the versatile applications mentioned above, we found that the input light wavelength is downconverted, or redshifted, at the output through such optical excitation transfers, as discussed shortly in Sec. II. This redshift may also be useful in various applications; for instance, it would effectively improve the sensitivity of a photodetector if the input wavelength could be shifted to longer wavelengths at which the photodetector is more sensitive. Applications to solar cells would also be one possibility.

In this paper, we describe our theoretical and experimental investigation of a system composed of a mixture of different-sized quantum dots involving optical near-field in-

teractions so that such a wavelength conversion is effectively induced. Based on a density-matrix formalism, we formulate the dynamics of a mixed quantum dot system where excitons generated in the smaller ones are transferred to larger ones via optical near-field interactions. We demonstrate that the ratio of the number of small quantum dots to large ones can be optimized so that the input light energy is efficiently transformed to the output energy. Experimental demonstrations are also shown using a mixture of 2 nm- and 2.8 nm-diameter CdSe/ZnS core/shell quantum dots randomly dispersed on a silicon photodiode surface where the effect of wavelength conversion is evaluated as induced photocurrents.

This paper is organized as follows. In Sec. II, we theoretically deal with a multiple quantum dot system composed of smaller and larger quantum dots. Section III summarizes our experimental demonstrations. Section IV concludes the paper.

II. OPTICAL EXCITATION TRANSFER IN MIXED SYSTEM OF DIFFERENT-SIZED QUANTUM DOTS: THEORY AND SIMULATION

We begin with the interaction Hamiltonian between an electron-hole pair and an electric field, which is given by

$$\hat{H}_{\text{int}} = - \int d^3r \sum_{i,j=e,h} \hat{\psi}_i^\dagger(\mathbf{r}) e \mathbf{r} \cdot \mathbf{E}(\mathbf{r}) \psi_j(\mathbf{r}), \quad (1)$$

where e represents a charge, $\hat{\psi}_i^\dagger(\mathbf{r})$ and $\hat{\psi}_j(\mathbf{r})$ are, respectively, creation and annihilation operators of either an electron ($i, j=e$) or a hole ($i, j=h$) at \mathbf{r} , and $\mathbf{E}(\mathbf{r})$ is the electric field.¹⁵ In usual light-matter interactions, $\mathbf{E}(\mathbf{r})$ is a constant since the electric field of diffraction-limited propagating light is homogeneous on the nanometer scale. Therefore, we can derive optical selection rules by calculating the dipole transition matrix elements. As a consequence, in the case of spherical quantum dots, for instance, only transitions to states specified by $l=m=0$ are allowed, where l and m are the orbital

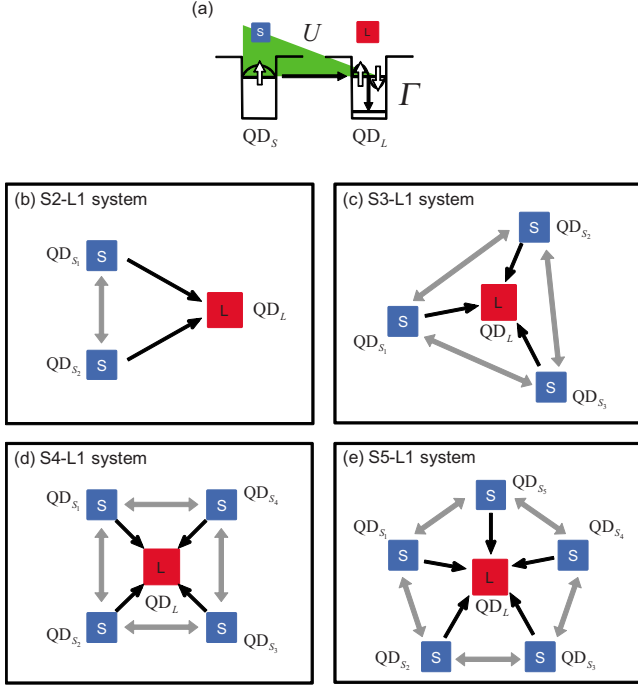


FIG. 1. (Color online) (a) Optical excitation transfer from a smaller quantum dot (QD_S) to a larger one (QD_L). (b) Three-dot system composed of two QD_Ss and one QD_L (S2-L1 system). (c) Four-dot system composed of three QD_Ss and one QD_L (S3-L1 system). (d) Five-dot system composed of four QD_Ss and one QD_L (S4-L1 system). (e) Six-dot system composed of five QD_Ss and one QD_L (S5-L1 system).

angular momentum quantum number and magnetic quantum number, respectively. In the case of optical near-field interactions, on the other hand, due to the large spatial inhomogeneity of the localized optical near fields at the surface of nanoscale material, an optical transition that violates conventional optical selection rules is allowed. Detailed theory can be found in Ref. 1.

Here we assume two spherical quantum dots whose radii are R_S and R_L , which we call QD_S and QD_L, respectively, as shown in Fig. 1(a). The energy eigenvalues of states specified by quantum numbers (n, l) are given by

$$E_{nl} = E_g + E_{ex} + \frac{\hbar^2 \alpha_{nl}^2}{2MR^2} \quad (n = 1, 2, 3, \dots), \quad (2)$$

where E_g is the band gap energy of the bulk semiconductor, E_{ex} is the exciton binding energy in the bulk system, M is the effective mass of the exciton, and α_{nl} are determined from the boundary conditions, for example, as $\alpha_{n0} = n\pi$, $\alpha_{11} = 4.49$. According to Eq. (2), there exists a resonance between the level of quantum number (1,0) of QD_S and that of quantum number (1,1) of QD_L if $R_L/R_S = 4.49/\pi \approx 1.43$. Note that the (1,1) level of QD_L is a dipole-forbidden energy level. However, optical near fields allow this level to be populated by excitation. Therefore, an exciton in the (1,0) level in QD_S could be transferred to the (1,1) level in QD_L. In QD_L, due to the sublevel energy relaxation with a relaxation constant Γ , which is faster than the near-field interaction, the

exciton relaxes to the (1,0) level, from where it radiatively decays. Also, the radiation lifetime of quantum dots is inversely proportional to their volume.¹⁶ Therefore, finally we find unidirectional optical excitation transfer from QD_S to QD_L. Here, we regard the optical excitation generated in QD_S as the *input* of the system and the radiation from QD_L as the *output*. Due to the energy dissipation (sublevel energy relaxation) in QD_L, the wavelength of the output light is redshifted relative to the input one.

We also consider a quantum dot system where multiple smaller dots (QD_S) can be coupled with one large dot (QD_L). Such a system composed of two QD_Ss and one QD_L, denoted by “S2-L1 system,” is shown in Fig. 1(b). Figure 1 also shows multiple quantum dot systems denoted by “S3-L1 system” [Fig. 1(c)], “S4-L1 system” [Fig. 1(d)], and “S5-L1 system” [Fig. 1(e)], which are respectively composed of three, four, and five QD_Ss connected to one QD_L. As schematically shown in Figs. 1(b)–1(e), we also assume interdot interactions between adjacent smaller quantum dots; that is, (i) QD_{S_i} interacts with QD_{S_{i+1}} ($i = 1, \dots, N - 1$) and (ii) QD_{S_N} interacts with QD_{S₁}, where N is the number of QD_Ss. We consider that such a ringlike arrangement of QD_Ss surrounding one QD_L is a reasonable assumption that represents a mixed system of multiple QD_S and one QD_L.

Now, what is of interest is maximizing the flow of excitons from these QD_Ss to the QD_L so that the wavelength conversion is effectively induced by controlling the mixture of QD_Ss and QD_L. We deal with such a problem theoretically based on a density-matrix formalism as described in the following.

We take the S2-L1 system [Fig. 1(b)] to describe the theoretical treatment. Figure 2(a) shows representative parametrizations associated with the S2-L1 system, where the two smaller dots are, respectively, QD_{S₁} and QD_{S₂}, and the larger dot is QD_L. The (1,0) levels in QD_{S_i} ($i = 1, 2$) are denoted by S_i and the (1,1) level in QD_L is denoted by L_2 . These three levels are resonant with each other and are connected by interdot interactions between QD_{S_i} and QD_L, denoted by $U_{S_i L}$, as well as interactions between the smaller dots QD_{S₁} and QD_{S₂}, denoted by $U_{S_1 S_2}$ in Fig. 2(a). The lower level in QD_L, namely, the (1,0) level, is denoted by L_1 , which could be filled via the sublevel relaxation denoted by Γ from L_2 . The radiations from the S_1 , S_2 , and L_1 levels are, respectively, represented by the relaxation constants γ_{S_1} , γ_{S_2} , and γ_{L_1} . We call the inverse of those relaxation constants the radiation lifetime in the following.

We suppose that the system initially has two excitons in S_1 and S_2 ; namely, the initial state of the system is represented by $|\phi_{S_1 S_2}\rangle = |1\rangle_{S_1} |0\rangle_{L_2} |0\rangle_{L_1} |1\rangle_{S_2}$, which is graphically represented in Fig. 2(b). With such an initial state, we can prepare a total of eleven bases, as summarized in Fig. 2(c), where zero, one, or two exciton(s) occupy the energy level(s) among S_1 , S_2 , L_1 , and L_2 . All bases are connected by either interdot interactions, radiative relaxations, or sublevel relaxations.

From the initial state, through the interdot interactions between the energy levels of [S_1 and L_2] and [S_2 and L_2], the excitons in S_1 and S_2 could respectively be transferred to L_2 . Also the exciton in S_1 could be transferred to S_2 through the

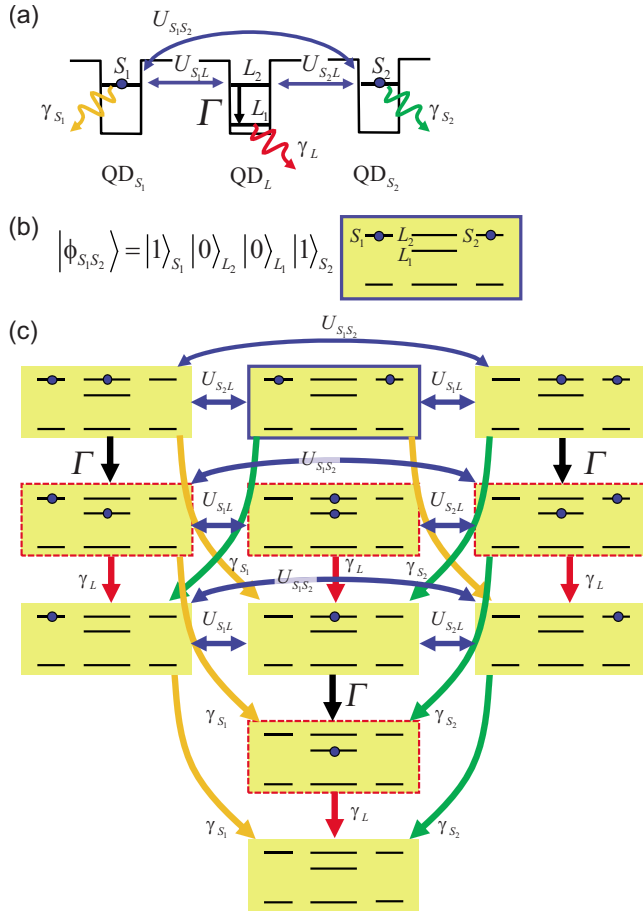


FIG. 2. (Color online) (a) Three-dot system composed of two smaller quantum dots (QD_{S_1} and QD_{S_2}) and a larger one QD_L . The $(1,0)$ level of QD_{S_i} (denoted by S_i) and the $(1,1)$ level of QD_L (denoted by L_2) are resonant and coupled by optical near-field interactions indicated by U_{S_iL} . The interaction between smaller dots is denoted by $U_{S_iS_j}$. The radiations from S_i and L_2 are denoted by γ_{S_i} and γ_L . The sublevel relaxation from L_2 to L_1 , the $(1,0)$ level of QD_L , is marked by Γ . (b) A graphical representation of the state of the system when the energy levels of S_1 and S_2 are respectively occupied with an exciton. (c) Total of 11 states where zero, one, or two exciton(s) occupy the energy level(s) in the system. Those states are interconnected via relaxations and interdot interactions.

interdot interaction between the smaller quantum dots and vice versa. Correspondingly, we can derive quantum master equations in the density-matrix formalism.^{1,17,18} The Hamiltonian regarding the two-exciton states, $|\phi_{S_1S_2}\rangle$, and $|\phi_{S_2L_2}\rangle$ is given by

$$H = \hbar \begin{pmatrix} \Omega_{S_1} + \Omega_{L_2} & U_{S_1L_2} & U_{S_1S_2} \\ U_{S_1L_2} & \Omega_{S_1} + \Omega_{S_2} & U_{S_2L} \\ U_{S_1S_2} & U_{S_2L} & \Omega_{S_2} + \Omega_{L_2} \end{pmatrix}, \quad (3)$$

where $\hbar U_{S_iL}$ is the near-field interaction between QD_{S_i} and QD_L , $\hbar U_{S_1S_2}$ is that between QD_{S_1} and QD_{S_2} , and $\hbar \Omega_{S_i}$ represents the eigenenergies of QD_{S_i} ($i=1,2$). The relaxation regarding those three states is given by

$$N_\Gamma = \begin{pmatrix} \frac{\gamma_{S_1} + \Gamma}{2} & 0 & 0 \\ 0 & \frac{\gamma_{S_1} + \gamma_{S_2}}{2} & 0 \\ 0 & 0 & \frac{\gamma_{S_2} + \Gamma}{2} \end{pmatrix}. \quad (4)$$

The Liouville equation for the system is then given by

$$\frac{d\rho(t)}{dt} = -i[H, \rho(t)] - N_\Gamma \rho(t) - \rho(t) N_\Gamma + \rho(t) P_\Gamma, \quad (5)$$

where P_Γ represents the relaxations that increase the corresponding population.¹⁷ (P_Γ is an empty matrix in the particular case described above.) Similarly, we can derive Liouville equations regarding the two-exciton states, one of which excitons fills L_1 , namely, $|\phi_{S_1L_1}\rangle$, $|\phi_{L_2L_1}\rangle$, and $|\phi_{S_2L_1}\rangle$, and also with one-exciton states $|\phi_{S_1}\rangle$, $|\phi_{L_2}\rangle$, and $|\phi_{S_2}\rangle$. Finally, we can calculate the population of the lower level of QD_L , which we regard as the output signal, as the summation of the populations of $|\phi_{S_1L_1}\rangle$, $|\phi_{S_2L_1}\rangle$, $|\phi_{L_2L_1}\rangle$, and $|\phi_{L_1}\rangle$, which correspond to states indicated by the dashed boxes in Fig. 2(c). In the numerical calculation, we assume $U_{S_iL}^{-1} = 200$ ps, $U_{S_iS_j}^{-1} = 100$ ps, $\Gamma^{-1} = 10$ ps, $\gamma_L^{-1} = 1$ ns, and $\gamma_{S_i}^{-1} = (R_L/R_S)^3 \times \gamma_L^{-1} \approx 2.92$ ns as a typical parameter set for the CdSe/ZnS quantum dots used for our experiments. The radiation lifetime of CdSe/ZnS quantum dots with a diameter of 2.8 nm, which is also used in the experiment in Sec. III, was measured to be 2.1 ns in Ref. 19, which is close to the above parametrization of radiation lifetimes. Also, the interaction time between smaller and larger quantum dots via optical near fields was estimated to be 135 ps in Ref. 19. Together with the fact that the interaction between the two dipole-allowed levels of the same-sized quantum dots, ($U_{S_iS_j}$), is stronger than that between smaller and larger dots, (U_{S_iL}),¹ we adopted the above parametrization for the interdot interactions. Finally, the calculated output population is represented by the curve A in Fig. 3(a).

Following the same procedure as described above, we can also derive quantum master equations for the S3-L1 system shown in Fig. 1(c), the S4-L1 system in Fig. 1(d), and the S5-L1 system in Fig. 1(e), with their initial states in which all smaller quantum dots have excitons. We can derive the evolution of the population of the lower level of the larger dot, that is, the output signal. We assume the same parameter sets in those systems as in the case of the S2-L1 system described above. The curves B–D in Fig. 3(a) respectively indicate the populations of the output signals from the S3-L1, S4-L1, and S5-L1 systems.

As the number of smaller quantum dots, or equivalently initial excitons, increases, the decay time of the output population from QD_L gets longer to accommodate multiple excitons initially located at QD_S . However, due to the limited radiation lifetime of QD_L ($\gamma_L^{-1} = 1$ ns), not all of the initial excitons can be successfully transferred to QD_L due to the state filling of the lower level of QD_L . Therefore, part of the

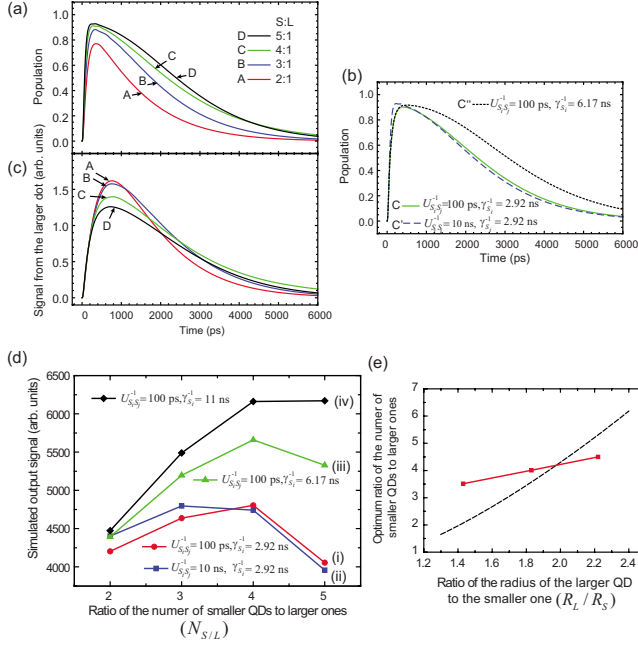


FIG. 3. (Color online) (a) Evolutions of the populations of the lower level of QD_L for the S2-L1, S3-L1, S4-L1, and S5-L1 systems in their initial states with all smaller dot(s) occupied by exciton(s). (b) Dependence of the output population on the interaction time between smaller dots ($U_{S_i S_j}^{-1}$) and the radiation lifetime of smaller dot ($\gamma_{S_i}^{-1}$). (c) Evolution of the output signals obtained by multiplying the population of the SN-L1 system obtained in (a) by a factor $\alpha/(N+1)$ so that the density of all quantum dots is kept constant. (d) Integrated signal levels obtained in (c) as a function of the ratio of the number of smaller QDs to larger ones (red circles). Their dependence on the interactions between smaller dots and the radiation lifetime of the smaller dots is also shown. (e) Optimal ratio of the number of smaller QDs to larger ones as a function of the ratio of the radius of the larger QD to the smaller one.

input populations must be decayed at QD_S , which results in loss in the conversion from the input to output.

One way of decreasing such loss is to increase the interdot interactions between smaller quantum dots, namely, $U_{S_i S_j}$, in order for an exciton to be transferred to neighboring smaller dots before being radiatively decayed. The curves C and C' in Fig. 3(b), respectively, indicate the output populations from two kinds of S4-L1 systems, in which $U_{S_i S_j}^{-1}$ is 100 ps and 10 ns. We find that the decay time of the output gets slightly longer with the greater interactions between smaller dots, ($U_{S_i S_j}^{-1}=100$ ps), than with weaker ones, ($U_{S_i S_j}^{-1}=10$ ns). In addition, the interactions between smaller dots play another interesting role in the system, tolerating system errors, as will be discussed shortly.

Another way of decreasing such loss is to give a longer radiation lifetime for the smaller dots ($\gamma_{S_i}^{-1}$), for instance, by decreasing the size of the smaller quantum dots while maintaining the conditions for optical excitation transfer from the smaller dots to the larger one. For instance, $\alpha_{12}=5.76$ in Eq. (2) satisfies the condition between the (1,0) level of QD_S and (1,2) level of QD_L when the size ratio of the quantum dots is given by $R_L/R_S=5.76/\pi \approx 1.83$. Such a configuration provides a longer radiation lifetime for QD_L , given by $\gamma_{S_i}^{-1}$

$= (R_L/R_S)^3 \times \gamma_L^{-1} \approx 6.17$ ns. This allows input excitons in QD_S to effectively wait until they can be transferred to the larger dot. The curve C'' in Fig. 3(b) indicates the output population with $\gamma_{S_i}^{-1}=6.17$ ns, where we can clearly observe a substantially enhanced output signal. Even smaller sizes for QD_S , such as corresponding to the condition $\alpha_{13}=6.99$ and $R_L/R_S=6.99/\pi \approx 2.22$, provide longer radiation lifetime of 11.0 ns, resulting in an enhanced output signal.

Now we consider quantum dot systems composed of different ratios of the number of smaller dots to larger ones while maintaining the total density of quantum dots constant. For this purpose, we multiply the output population from the SN-L1 system by a factor $\alpha/(N+1)$, where N represents the number of smaller quantum dots connected to one larger dot. The factor α indicates the number of quantum dots, regardless of their size (smaller or larger), in a given unit area. Figure 3(c) shows the resulting signals from SN-L1 systems, each of which was already obtained as shown in Fig. 3(a). The unit on the vertical axis in Fig. 3(c) is arbitrary; we assumed $\alpha=10$ in Fig. 3(c).

By integrating the time evolutions of these output signals between 0 and 20 ns, the resultant signal (that is, the integrated output signal) can be compared as shown by the circles (i) in Fig. 3(d). They exhibit their maximum when the ratio of the number of smaller dots to the larger one, which we denote as $N_{S/L}$, is 4. We can clearly see that increasing the number of smaller quantum dots does not necessarily contribute to increased output signal. Besides the ratio of the number of smaller dots to larger ones, the output signal also depends on the interactions between the smaller dots and the radiation lifetime of the smaller dots, as already discussed above. Figure 3(d) also includes the estimated output signal level with a $U_{S_i S_j}^{-1}$ value of 10 ns, as indicated by the squares (ii), where the optimal mixture of QD_S and QD_L that yields the highest output signal, or equivalently, that most efficiently induces the wavelength conversion, is obtained when $N_{S/L}$ is 3. With longer radiation lifetime of the smaller quantum dots, $\gamma_{S_i}^{-1}=6.17$ ns and $\gamma_{S_i}^{-1}=11.0$ ns, the output signal levels are greatly improved, as respectively indicated by the triangles (iii) and diamonds (iv) in Fig. 3(d).

Two remarks should be made regarding these theoretical calculations. First, the optimal ratios of the number of smaller quantum dots to larger ones in the cases $R_L/R_S=1.43$ [circles (i)] and $R_L/R_S=1.83$ [triangles (iii)] are both obtained when $N_{S/L}$ is 4, as shown in Fig. 3(d). However, with the larger quantum dot size ratio R_L/R_S of 1.83, that is $\gamma_{S_i}^{-1}=6.17$ ns, the output signal remains larger even when $N_{S/L}$ is 5. For the case of $R_L/R_S=2.22$ [diamonds (iv)], the output signal is nearly equal when $N_{S/L}$ is both 4 and 5. In order to account for this tendency, we evaluate the optimal $N_{S/L}$ by calculating the weighted center with respect to $N_{S/L}$ that yields output signals greater than 0.9 of the maximum. Then, we can clearly observe that the optimal ratio of the number of smaller QDs to larger ones increases as the ratio of the radius of the larger QD to the smaller one (R_L/R_S) increases, as indicated by the squares in Fig. 3(e).

We can understand these phenomena from the following reasoning. The larger quantum dot could accommodate multiple input excitations from smaller quantum dots as long as

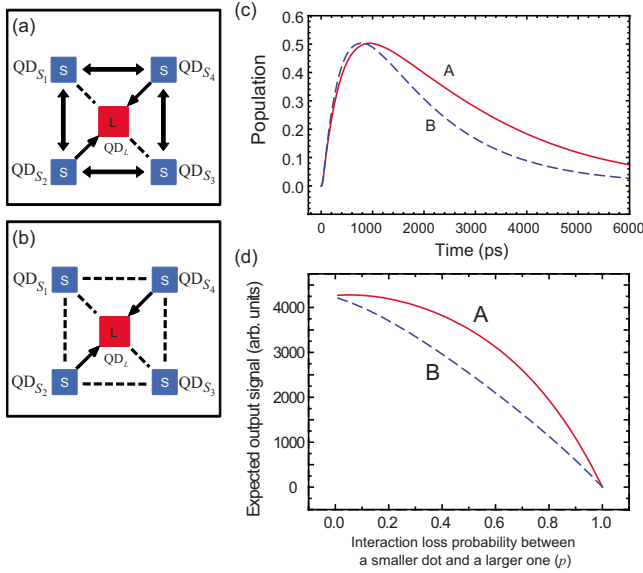


FIG. 4. (Color online) (a) A S4-L1 system in which the interactions between $[QD_{S_1}$ and $QD_L]$ and $[QD_{S_3}$ and $QD_L]$ are degraded. (b) A S4-L1 system where the interactions between smaller dots are also degraded. (c) Evolution of populations of the radiation from the larger dot in the system shown in (a) [curve A] and (b) [curve B]. (d) Expected output signal from S4-L1 systems with and without inter-smaller-dot interactions as a function of interaction-loss probability between a smaller dot and a larger one.

the input excitation can effectively wait at the smaller quantum dot. Therefore, the larger quantum dot could ideally accommodate multiple excitations, at most $\gamma_S^{-1}/\gamma_L^{-1}=(R_L/R_S)^3$. However, due to the finite interaction time between QD_S and QD_L (U_{SL}^{-1}), it is approximately limited by $\gamma_S^{-1}/(\gamma_L^{-1}+NU_{SL}^{-1})$, where N represents the number of excitations in the smaller quantum dots. Therefore, the number of smaller quantum dots whose excitations are all accommodated in the larger one will be approximately given by solving the equation

$$N = \frac{\gamma_S^{-1}}{\gamma_L^{-1} + NU_{SL}^{-1}} = \frac{(R_L/R_S)^3 \gamma_L^{-1}}{\gamma_L^{-1} + NU_{SL}^{-1}}. \quad (6)$$

The dashed curve in Fig. 3(e) depicts N obtained by solving Eq. (6) as a function of R_L/R_S , assuming $\gamma_L^{-1}=1$ ns and $U_{SL}^{-1}=200$ ps, which agrees with the optimal ratio of the number of the smaller QDs to large ones indicated by the squares in Fig. 3(e), which are obtained via the numerical evaluations shown in Fig. 3(d).

The second remark is to highlight another function of the interactions between smaller dots. Figure 4(a) schematically represents an S4-L1 system where four smaller dots surround one larger dot and there are interdot interactions between adjacent smaller dots. Here, we suppose that some of the interactions between the smaller dots and the larger one are degraded or lost. Such a weak interaction could physically correspond to situations, for instance, where the distance between the smaller dot and the larger one is very large, or the size or the shape of the quantum dots deviates from the required conditions for energy transfer, or other reasons. In Fig. 4(a), we suppose that QD_{S_1} and QD_{S_3} have extremely

weak interactions with QD_L ; the dashed lines in Fig. 4(a) schematically indicate those weak interactions. Also, Fig. 4(b) represents another S4-L1 system where *all* of the interactions between smaller dots are assumed to be negligible, in addition to the weak interactions assumed in the system in Fig. 4(a). What is of interest is to evaluate the impact of the interactions between smaller dots on the energy transfer from the smaller dots to the larger one as a total system. In the following analysis, we assume degraded interactions that are 100 times weaker than the normal ones.

The curves A and B in Fig. 4(c), respectively, represent the evolutions of the population of the radiation from the larger dot in the system shown in Figs. 4(a) and 4(b), where the former exhibits a higher population compared with the latter. In the system shown in Fig. 4(a), thanks to the interactions between smaller dots, the excitations in QD_{S_1} and QD_{S_3} can be successfully transferred to QD_L by way of the adjacent smaller dots. On the other hand, it is hard for the excitations in QD_{S_1} and QD_{S_3} in Fig. 4(b) to be transferred to QD_L due to the weak interactions with the surrounding dots. From a system perspective, the interactions among smaller dots provide *robustness* to degradation of the excitation transfer from the smaller dots to larger ones.

To quantitatively evaluate such robustness, here we introduce the probability that an interaction between a smaller dot and a larger one suffers interaction degradation or loss; we denote it by p ($0 \leq p \leq 1$). Accordingly, we assume that the probability of the existence of interaction between a smaller and a larger one is given by $1-p$. We consider that although modeling of the loss in such an interaction is simple, that is, the probability p indicates the loss/existence of the interactions, one can clearly grasp the role of interactions in the following discussion. We can calculate the probability of all possible resulting system configurations as a function of p ; for instance the probability of the system shown in Fig. 4(a) is given by $p^2(1-p)^2$. Also, we calculate the evolution of the population and its integral as the output signal for each of the system configurations. Finally, we can derive the expected output signal level as a function of p , given by

$$E(p) = \sum_i P(C_i) L(C_i), \quad (7)$$

where C_i indicates each system configuration, $P(C_i)$ means the probability of resulting in system C_i , and $L(C_i)$ means the output signal level from system C_i .

The curves A and B in Fig. 4(d), respectively, represent the expected output signals corresponding to systems with and without interactions between smaller dots as a function of the interaction loss probability between a smaller dot and a larger one. We can clearly observe that the expected output signal levels remain higher thanks to the existence of interactions between smaller dots, even though they suffer a larger p ; this is a manifestation of the improved robustness of the system provided by the interactions between smaller dots.

III. EXPERIMENTS

In order to verify the effect of wavelength conversion via different sized quantum dots involving near-field interactions

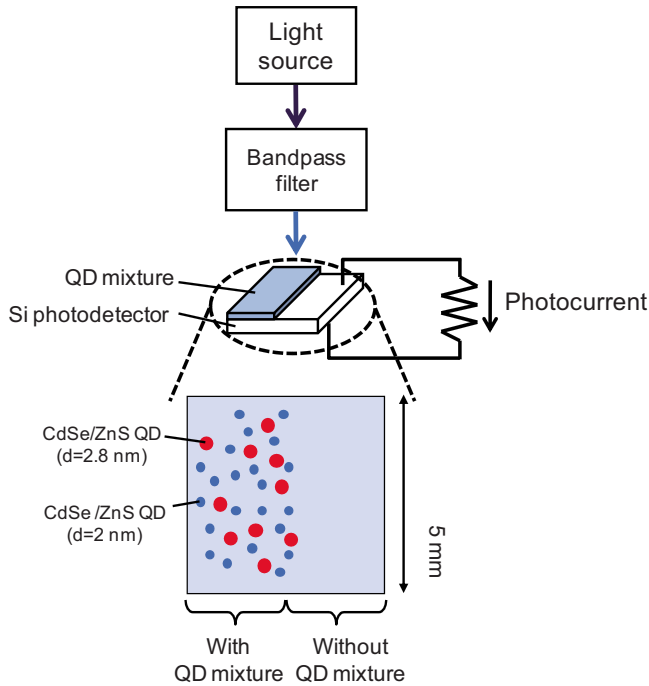


FIG. 5. (Color online) Experimental devices and setups used for the characterization of induced photocurrents.

and its impact on the increased sensitivity in light detection, we experimentally fabricated a composition of quantum dots formed on the surface of a photodiode by the following procedure.

Two kinds of quantum dots, QD_S and QD_L , were both CdSe/ZnS core/shell quantum dots (Evident Technologies, Inc., Core Shell EviDots). The diameters of QD_S and QD_L were respectively 2.0 nm and 2.8 nm. Note that the ratio of the radii of those dots is 1.43, which is the condition discussed in Sec. II. The quantum dots were dispersed in a matrix composed of toluene and ultraviolet curable resin and coated on the surface of a silicon photodiode whose aperture was $5.8 \text{ mm} \times 5.8 \text{ mm}$ (Hamamatsu Photonics K.K., Si Photodiode S2368). The mean density of the quantum dots was kept constant so that the mean distance between quantum dots was around 40 nm. As schematically shown in Fig. 5, half of the surface of the photodiode was spin-coated by an ultraviolet-curable resin with a mixture of quantum dots and cured by ultraviolet radiation for 10 min, whereas the other half of the surface was coated by the same resin without the quantum dot mixture. Input light was selectively radiated onto each area to evaluate the difference in the generated photocurrent.

The light source was composed of a deuterium lamp and a halogen lamp. The emitted light was spectrally filtered in 2 nm wavelength intervals using a grating installed in a spectrometer and was radiated onto the sample. The diameter of the light spot on the sample was around 1 mm. The induced photocurrent was measured with a lock-in amplifier connected in parallel to an external load resistor of the photodiode. The experiment was performed at room temperature.

The ratio of the increased photocurrent at each wavelength between 300 and 400 nm is evaluated as $[I_w(\lambda)$

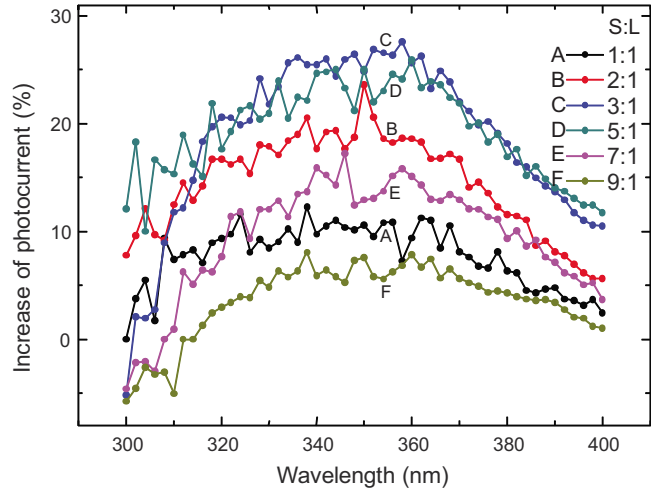


FIG. 6. (Color online) Increase in the photocurrent with different mixtures of smaller and larger quantum dots as a function of input light wavelength.

$-I_{wo}(\lambda)]/I_{wo}(\lambda)$, where $I_w(\lambda)$ and $I_{wo}(\lambda)$, respectively, indicate the photocurrents induced by input light with wavelength λ irradiating the areas with and without the mixture of quantum dots. Here we attribute the increase in such a metric to optical excitation transfer between quantum dots by which the input wavelength is redshifted to wavelengths where the photodetector is more sensitive.

Figure 6 shows the increase in the induced photocurrent as a function of the input light wavelength. The ratio of the number of QD_S to QD_L was controlled to be $N_{S/L}=1, 2, 3, 5, 7$, and 9 , which are respectively indicated by the curves A–F in Fig. 6, while the total density of the quantum dots was kept constant. The increase in the photocurrent was observed to be higher when the ratio of the number of QD_S to QD_L was 3:1. The squares in Fig. 7 represent the average increase in the photocurrent between 340 and 360 nm in Fig. 6, showing a maximum when the ratio of the number of QD_S to QD_L was 3:1. This agrees with the theoretical optimal ratio of the

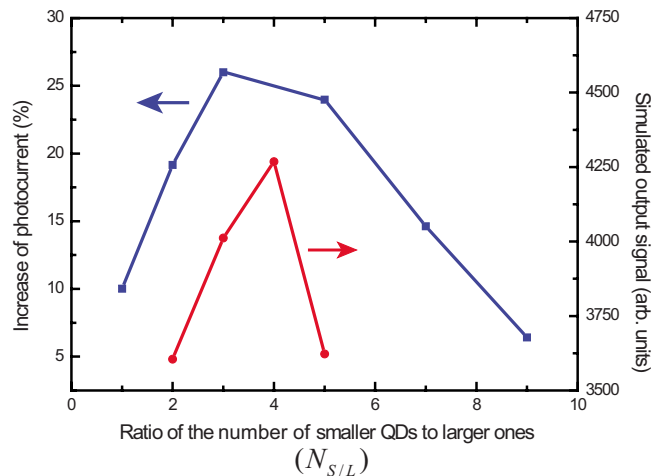


FIG. 7. (Color online) The average increase in photocurrent as a function of the ratio of the number of smaller quantum dots to larger ones (squares), which agrees with theoretical calculations (circles).

number of smaller quantum dots to larger ones discussed in Sec. II, indicated by the circles in Fig. 7, with parameters $U_{S_i S_j}^{-1} = 100$ ps, $U_{S_i L}^{-1} = 200$ ps, $\gamma_L^{-1} = 1$ ns, and $\gamma_{S_i}^{-1} = 2.92$ ns, which is also shown by the circles (i) in Fig. 3(d). More detailed investigation of each of the parameters, such as the radiation lifetime of CdSe quantum dots reported for instance in Refs. 20 and 21, could result in better agreement. Nevertheless, as demonstrated by the squares in Fig. 3(e), the optimal ratio of smaller dots to larger ones should be around 4, which agrees with the experimental data shown in Fig. 7.

IV. CONCLUSION

We theoretically and experimentally investigated a system composed of a mixture of different-sized quantum dots involving optical near-field interactions so that optical excitation transfer is effectively induced. Based on the density-matrix formalism, we formulated a quantum dot mixture in which excitons generated in the smaller ones are transferred to the larger one. The evolution of the population was evaluated as a function of the number of smaller quantum dots interacting with a larger one. We demonstrated that the ratio of the number of smaller quantum dots to larger ones could be optimized so that the input light energy was efficiently transferred to the output. The effects of interactions between smaller dots and the radiation lifetime of the smaller dots

were also analyzed. We also demonstrated that the interactions between smaller quantum dots provide robustness against degradation of the interactions between the larger and the smaller dots. Experimental demonstrations are shown based on a mixture of CdSe/ZnS core-shell quantum dots dispersed on the surface of a silicon photodiode. The induced photocurrent was maximized when the ratio of the number of smaller quantum dots to larger ones was 3, which agrees with theoretical calculations.

We will seek further theoretical and experimental insights regarding such optical excitation transfer which is enabled uniquely by optical near-field interactions, in order to allow a wide range of system applications, as well as a deeper understanding of light-matter interactions on the nanometer scale.

ACKNOWLEDGMENTS

The authors would like to thank Kiyoshi Kobayashi of the University of Yamanashi and Masaru Tsukada and Hiroyuki Tamura of Tohoku University for helpful discussions on the theory of optical excitation transfer. This work was partially supported by the New Energy and Industrial Technology Development Organization (NEDO) under the program of comprehensive activity for personnel training and industry-academia collaboration based on NEDO projects.

-
- ¹M. Ohtsu, K. Kobayashi, T. Kawazoe, T. Yatsui, and M. Naruse, *Principles of Nanophotonics* (Taylor & Francis, Boca Raton, 2008).
- ²P. Vasa, R. Pomraenke, S. Schwieger, Yu. I. Mazur, V. Kunets, P. Srinivasan, E. Johnson, J. E. Kihm, D. S. Kim, E. Runge, G. Salamo, and C. Lienau, *Phys. Rev. Lett.* **101**, 116801 (2008).
- ³*Semiconductor and Metal Nanocrystals*, edited by V. I. Klimov (Marcel Dekker, New York, 2003).
- ⁴*Near Field Optics*, edited by D. W. Pohl and D. Courjon (Kluwer Academic, Dordrecht, 1993).
- ⁵M. Naruse, T. Kawazoe, T. Yatsui, S. Sangu, K. Kobayashi, and M. Ohtsu, in *Progress in Nano-Electro-Optics V*, edited by M. Ohtsu (Springer, Berlin, 2006).
- ⁶T. Kawazoe, K. Kobayashi, J. Lim, Y. Narita, and M. Ohtsu, *Phys. Rev. Lett.* **88**, 067404 (2002).
- ⁷M. Ohtsu, T. Kawazoe, T. Yatsui, and M. Naruse, *IEEE J. Sel. Top. Quantum Electron.* **14**, 1404 (2008).
- ⁸Y. Tanaka and K. Kobayashi, *J. Microsc.* **229**, 228 (2008).
- ⁹T. Kawazoe, K. Kobayashi, K. Akahane, M. Naruse, N. Yamamoto, and M. Ohtsu, *Appl. Phys. B: Lasers Opt.* **84**, 243 (2006).
- ¹⁰T. Yatsui, H. Jeong, and M. Ohtsu, *Appl. Phys. B: Lasers Opt.* **93**, 199 (2008).
- ¹¹T. Kawazoe, K. Kobayashi, S. Sangu, and M. Ohtsu, *Appl. Phys. Lett.* **82**, 2957 (2003).
- ¹²T. Yatsui, S. Sangu, T. Kawazoe, M. Ohtsu, S. J. An, J. Yoo, and G.-C. Yi, *Appl. Phys. Lett.* **90**, 223110 (2007).
- ¹³H. Imahori, *J. Phys. Chem. B* **108**, 6130 (2004).
- ¹⁴S. Kang, T. Umeyama, M. Ueda, Y. Matano, H. Hotta, K. Yoshida, S. Isoda, M. Shiro, and H. Imahori, *Adv. Mater.* **18**, 2549 (2006).
- ¹⁵H. Haug and S. W. Koch, *Quantum Theory of the Optical and Electronic Properties of Semiconductors* (World Scientific, Singapore, 2004).
- ¹⁶T. Itoh, M. Furumiya, T. Ikehara, and C. Gourdon, *Solid State Commun.* **73**, 271 (1990).
- ¹⁷H. J. Carmichael, *Statistical Methods in Quantum Optics I* (Springer-Verlag, Berlin, 1999).
- ¹⁸M. Naruse, T. Miyazaki, F. Kubota, T. Kawazoe, K. Kobayashi, S. Sangu, and M. Ohtsu, *Opt. Lett.* **30**, 201 (2005).
- ¹⁹W. Nomura, T. Yatsui, T. Kawazoe, and M. Ohtsu, *J. Nanophotonics* **1**, 011591 (2007).
- ²⁰S. A. Crooker, T. Barrick, J. A. Hollingsworth, and V. I. Klimov, *Appl. Phys. Lett.* **82**, 2793 (2003).
- ²¹O. Labeau, P. Tamarat, and B. Lounis, *Phys. Rev. Lett.* **90**, 257404 (2003).